



Biodegradable metabotissugenic citrate-based polymer derived self-sealing pro-regenerative membrane for tendon anti-biofouling and repair

Changhao Han^{a,1} , Lujiao Zhang^{b,1} , Rong Bao^a , Yutong Lu^b , Xinpeng Dong^a , Tianyi Zhang^a , Yuanhao Yang^a , Yao Xiao^a , Liangxuan Fu^a , Pusheng Guo^a , Jian Yang^{b,c,d,**} , Shen Liu^{a,*} 

^a Department of Orthopaedics, Shanghai Sixth People's Hospital Affiliated to Shanghai Jiao Tong University School of Medicine, 600 Yishan Rd, Shanghai, 200233, PR China

^b Department of Materials Science and Engineering, Westlake University, Hangzhou, Zhejiang, 310030, PR China

^c Research Center for Industries of the Future, Westlake University, Hangzhou, Zhejiang, 310030, PR China

^d Center for Biobased Materials, Muiyuan Laboratory, 110 Shangding Road, Zhengzhou, 450016, Henan Province, PR China

ABSTRACT

Tendon stem/progenitor cells (TSPCs) are crucial for intrinsic regeneration of injured tendons which consume a substantial amount of energy relying on the tricarboxylic acid (TCA) cycle. Citric acid, the key substrate of the TCA cycle, emerges as a promising candidate for regulating energy metabolism. However, sustainable methods in providing energy metabolic substrates across the whole regenerating process has been neglected. Herein, a metabotissugenic membrane consisting of poly(octamethylene citrate) and L-lysine diisocyanate, POCL₁₀, was developed to consistently biodegrade and provide citrate substrates. Furthermore, the POCL₁₀ membrane exhibited self-sealing properties due to the introduction of strong hydrogen bonds and demonstrated anti-biofouling capacity in vitro. Intriguingly, POCL₁₀ showed excellent regenerative capability by promptly upregulating TSPC proliferation, energy metabolism and differentiation. In vivo, POCL₁₀ was effortlessly wrapped around the injured Achilles tendon showcasing with anti-tissue adhesion and prominent collagen organization along with strengthened biomechanical properties. Hence, the development of POCL expands the reservoir of available biodegradable citrate-based biomaterials and provides a unique metabotissugenic biomaterial platform for tendon anti-biofouling and repair.

1. Introduction

Tendon injuries, particularly Achilles tendon ruptures, are among the most prevalent musculoskeletal injuries, significantly impacting patients' mobility and quality of life [1–3]. Despite advancements in surgical techniques and rehabilitation protocols, postoperative adhesion formation (PAF) remains a major complication following tendon repair surgeries, often leading to impaired tendon function and patient dissatisfaction [4]. The formation of adhesions is a multifactorial process, primarily driven by an imbalance between intrinsic and extrinsic tendon healing mechanisms. Intrinsic healing involves the proliferation and differentiation of tenocytes within the tendon, while extrinsic healing is characterized by the infiltration of inflammatory cells and fibroblasts from the surrounding tissues [5,6]. Exogenous healing leads to impaired biomechanical functions which reduces the tendon's role of

weight bearing. Factors such as excessive inflammation, inappropriate mechanical loading, and the upregulation of specific growth factors like transforming growth factor- β (TGF- β) have been identified as key contributors to adhesion formation [7–10].

To address this challenge, various strategies have been explored to prevent or minimize postoperative adhesion formation. Studies have demonstrated that the use of biomaterials to create physical barriers combined with controlled drug release can inhibit the proliferation of peritendinous tissue cells and block extrinsic healing [11–13]. For example, foreign products such as SurgiWrap [14], Interceed TC7 [15], and Seprafilm [16], as well as domestic products like the Súbikang™ polysaccharide bioadhesive, have all shown good anti-adhesion effects. However, these anti-adhesion materials often need to be sutured in place, which increases the difficulty of surgery, the risk of infection, and the possibility of material displacement. Moreover, existing

Peer review under the responsibility of editorial board of Bioactive Materials.

* Corresponding author.

** Corresponding author. Department of Materials Science and Engineering, Westlake University, Hangzhou, Zhejiang, 310030, PR China.

E-mail addresses: deffaron98@sjtu.edu.cn (C. Han), zhanglujiao@westlake.edu.cn (L. Zhang), bao-rong@sjtu.edu.cn (R. Bao), luyutong@westlake.edu.cn (Y. Lu), dongxinpen@sjtu.edu.cn (X. Dong), dayone618@sjtu.edu.cn (T. Zhang), yangyuanhao1021@sjtu.edu.cn (Y. Yang), xiaoyao715@shsmu.edu.cn (Y. Xiao), fulx666@sjtu.edu.cn (L. Fu), gps760311@sjtu.edu.cn (P. Guo), yangjian07@westlake.edu.cn (J. Yang), liushensjtu@sjtu.edu.cn (S. Liu).

¹ These authors contributed equally.

<https://doi.org/10.1016/j.bioactmat.2025.05.020>

Received 2 April 2025; Received in revised form 16 May 2025; Accepted 18 May 2025

Available online 28 May 2025

2452-199X/© 2025 The Authors. Publishing services by Elsevier B.V. on behalf of KeAi Communications Co. Ltd. This is an open access article under the CC BY-NC-ND license (<http://creativecommons.org/licenses/by-nc-nd/4.0/>).

anti-adhesion materials have limitations: traditional degradable synthetic polymers, such as polylactic acid (PLA), polyglycolic acid (PGA), and polycaprolactone (PCL), lack regenerative properties, and their degradation products may exacerbate inflammation [17–20]. Natural biomaterials, such as hyaluronic acid (HA)-based hydrogels, degrade too quickly, increasing the risk of anti-adhesion failure. Therefore, the development of new anti-adhesion materials with good biocompatibility, self-sealing properties (sutureless closure), degradability, and the ability to promote tissue regeneration is an urgent and important issue.

Yang et al. pioneered the development of a series of citrate-based biomaterials for various regenerative engineering applications [21]. Notably, the recent US Food and Drug Administration (FDA) clearance of the biodegradable poly(octamethylene citrate) (POC)/hydroxyapatite-based orthopedic fixation devices for use in humans represents a translational research milestone in biomaterial science [22]. POC can serve as a carrier material that releases citric acid through degradation. Citric acid, as an intermediate of cellular metabolism, is transported to the cytoplasm via the mitochondrial citrate carrier (CIC, SLC25A1), where it is converted into acetyl-CoA and oxaloacetate. This process regulates fatty acid and lipid synthesis as well as protein acetylation, thereby enhancing protein stability and promoting cell division and proliferation. In the nucleus, citric acid is converted into acetyl-CoA to regulate histone acetylation, which in turn modulates epigenetic modifications and gene expression [23–27]. In previous studies, we have proved that exogenous citric acid could promote intracellular ATP generation, regulate the regenerative microenvironment, enhance vascular and nerve regeneration, and promote stem cell metabonegenic (metabolic + osteogenic) differentiation [28]. Drawing on the multifaceted roles that citrate plays in orchestrating intracellular metabolic pathways to drive tissue regeneration by coordinating the functions of various cell types integral to the regenerative process of tissues such as blood vessels, nerves, skin, bone, and so on, we then extended the concept of “metabonegenesis” to “metabotissugeneis” [22]. Understanding citrate’s metabotissugenic function will inform and inspire the design of next-generation citrate-based biomaterials. However, the role of citrate for tendon repair and regeneration has not previously been studied yet.

Tendon stem cells predominantly rely on glycolysis under homeostatic states which consume a minimal amount of energy [29]. However, upon injury, a transition from a low to high energy producing state occurs to meet the energy consuming standards of tissue healing [30–32]. Tendon regeneration comprises three main processes: inflammation, proliferation and remodeling. During the proliferative phase, resident tendon stem/progenitor cells (TSPCs) proliferate, differentiate and deposit extracellular matrix (ECM) to replace the impaired tissue [33]. These processes require a higher energy-producing pathway, which depends on the citric acid (tricarboxylic acid, TCA) cycle and oxidative phosphorylation (OXPHOS). It was reported that TCA cycle is substantial for tendon recovery [34]. Moreover, exogenous TSPC delivery to injured tissues also displayed a transcriptional enrichment in citrate cycle and OXPHOS pathways, indicating the importance of high energy-producing metabolic processes in tendon regeneration [35]. Enhanced TSPC development in vivo further facilitates tendon mechanical properties [36]. However, the application of a systemic inhibitor or the implantation of stem cells may lead to various side effects, including off-target effects and unstable cell function [37–39]. As exogenous citrate induces stem cell energy production and metabotissugeneis, development of a citrate-based polymer with high biocompatibility for tendon injury implantation is highly desirable.

Given the pro-regenerative potential of metabotissugenic citrate-based biomaterials, it is intriguing to explore the potential role in promoting tendon regeneration. This area has not been extensively studied. Herein, we have meticulously designed the molecular structure of a POC-based membrane material. For the first time, we have developed a novel anti-biofouling material based on citric acid that integrates multiple functions, including degradability, self-sealing, mechanical

matching, and metabolic regulation, specifically tailored for anti-biofouling and tendon repair. We achieved this by crosslinking POC with L-Lysine Diisocyanate (LDI) to fabricate POCL membranes with a thickness of approximately 100 μm (Fig. 1). As a bio-based isocyanate, LDI offers several distinct advantages: (1) enhancing biocompatibility and controlled degradation rate to create a conducive environment for repair; (2) providing flexible crosslinking molecular chains that render a membrane with thinner and mechanically matched modulus with tissues in the implanted region, which reduces foreign body sensation and minimizes inflammatory reactions; (3) introducing hydrogen-bonding sites, imparting the membrane with self-sealing properties. We hypothesize that the controlled release of citrate increases biocompatibility with TSPCs and the degradable POCL membrane provides a physical anti-biofouling barrier against PAF. Moreover, cytosol influx of citrate would induce a metabolic shift as OXPHOS regulated energy metabolism promotes TSPC development and improve mechanical properties in vivo. Overall, this work represents a new direction in addressing the significant clinical challenges in tendon anti-biofouling and repair.

2. Results and discussion

2.1. Synthesis and characterization of the citrate-based membrane

The POC prepolymer (pre-POC) was synthesized (Fig. S1) and structurally characterized by ^1H NMR and mass spectrometry (Fig. S2). Subsequently, the pre-POC was chemically crosslinked using LDI, which possesses flexible molecular chains. By varying the proportion of LDI, a series of POCL_x membranes (where x denotes different LDI ratios) were prepared, with LDI contents of 0 %, 5 %, 10 %, 15 %, and 20 %, respectively. POCL_x membranes had a transparent feature and were highly flexible when bent by forceps (Fig. 2A). The morphological images observed through scanning electron microscopy (SEM) showed that all POCL_x membranes presented with a dense texture and smooth surface (Fig. 2B). The non-porous structure could inhibit the infiltration and adhesion of cells [40]. The lateral view displayed that pure POC membranes were approximately $136.78 \pm 4.63 \mu\text{m}$ thick. With the crosslinking of LDI, the thickness of $\text{POCL}_{5/10/15/20}$ membranes decreased to $102.59 \pm 1.13 \mu\text{m}$, $100.66 \pm 1.27 \mu\text{m}$, $100.07 \pm 1.55 \mu\text{m}$, and $99.75 \pm 1.00 \mu\text{m}$, respectively. (Fig. 2C, D and Table S1). Crosslinking resulted in a further increase in the membrane’s density, which could enhance its barrier properties. The reduced thickness of biomaterials could also decrease the foreign body sensation upon implantation [41]. Furthermore, the hydrophobicity of POCL_x membranes were tested by water contact angle (WCA) analysis. The POC membrane exhibited hydrophobicity due to the presence of the hydrophobic alkyl chains in 1, 8-octanediol (OD). Crosslinking increases the membrane’s density, which typically resulted in an increased water contact angle, indicating enhanced hydrophobicity. However, LDI is a bio-based isocyanate that contains hydrophilic groups. As the amount of LDI incorporated into the membrane increases, the water contact angle decreased slightly. Despite this, the overall hydrophobic nature of the POCL_x were maintained due to the dominant presence of hydrophobic components (Fig. 2E). FTIR spectrometer analysis (in the range of $400\text{--}4000 \text{ cm}^{-1}$) was addressed to further examine the extent of POCL_x crosslinking. The stretching vibration peak of the ester bond ($-\text{COOH}-$) is the main feature of POC synthesis observed at 1749 cm^{-1} , while the amido bond ($-\text{CONH}-$) that peaks at 1531 cm^{-1} marked the characteristic of LDI crosslinking (Fig. 2F). As highlighted in green, the peak corresponding to the amido bond exhibited a corresponding increase with the increase in the amount of LDI used. The FTIR spectra display signals at $3300\text{--}3500 \text{ cm}^{-1}$, which is characteristic of the $-\text{OH}$ group. As the amount of LDI increases, the cross-linking density of the film also increases. This leads to a reduction in the number of residual hydroxyl groups. Consequently, the peak intensity at $3300\text{--}3500 \text{ cm}^{-1}$ decreases accordingly. This trend was consistently observed in the X-ray photoelectron spectroscopy (XPS)

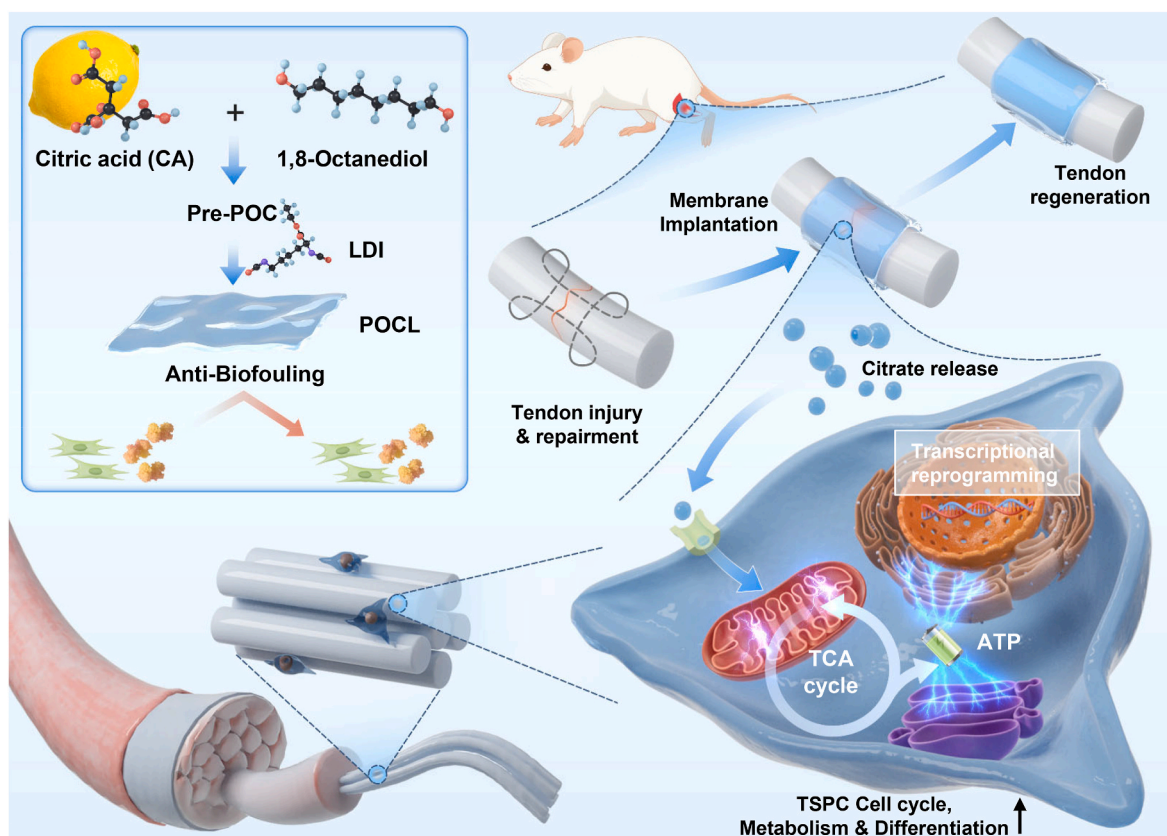


Fig. 1. Schematic diagram illustrating the metabiotissugenic effect of the degradable citrate-based membrane for anti-biofouling and tendon regeneration.

analysis. Specifically, the N 1s peak and the C-N/C binding ratios showed significant increases from 0 % to 5.62 %, 6.89 %, 13.64 %, and 18.83 %, respectively (Fig. 2G, H, Fig. S3 and Table S1). Therefore, we could conclude that as the amount of LDI increases, the hydrogen bonding interactions of $POCL_x$ also increase accordingly. The degradation behavior of the $POCL_x$ were assessed in both PBS and esterase solutions (0.05 mg/mL). The results indicated that in pure PBS, POC degraded at the fastest rate. As the amount of LDI incorporated increases, the crosslinking density of the membrane material also increased, leading to a corresponding decrease in the degradation rate (Fig. 2I). In contrast, the introduction of LDI enhanced the ester bond content within the membrane material. Therefore, in the esterase-containing degradation solution, membranes with higher crosslinking density degraded more rapidly (Fig. S4). Concentration of CA released by $POCL_x$ membranes in PBS were also tested, as concentrations decreased with the increase of LDI crosslinking (Fig. 2J). This observation demonstrated that the incorporation of LDI could modulate the degradation rate of the material, thereby controlling the release rate of citric acid and, consequently, the biocompatibility of the membrane material.

2.2. Mechanical properties and self-sealing capacity of $POCL_x$ membranes

. Modulus matching of materials with tissue reduces immunological rejection [42]. The implanted membrane materials should possess good flexibility to match the mechanical properties of the tissues. This ensures that the materials can conform to the tissue's mechanical strength without causing excessive stress or damage. Therefore, the modulus of the native tendon, full-length hind limb skin and muscle surrounding the tendon was primarily tested. Results show that the modulus of the tissues were around 340.05 ± 107.17 MPa, 72.87 ± 20.26 MPa and 0.26 ± 0.10 MPa, respectively (Fig. S5). Furthermore, the membranes were examined showing the tensile strength (approximately 0–120 KPa)

lower than the modulus of tissues which allowed membranes to be easily bended and maintain a soft contact with muscular tissues (Fig. 3A and Table S1). The selected crosslinking agent LDI possesses flexible molecular chains, which allow the membrane material to maintain good flexibility while increasing its density. This dual benefit is crucial for reducing foreign body inflammatory responses. Flexible molecular chains can enhance the material's adaptability to biological tissues, minimizing the mechanical mismatch that often leads to inflammation. Currently, the anti-biofouling membranes used in clinical practice require additional suturing during application, which significantly increases the complexity of the procedure and the risk of infection. Therefore, membranes with self-sealing properties are more suitable for clinical use. To more intuitively demonstrate the self-adhesive properties of the membrane material, we wrapped it around a finger and performed continuous bending. The results showed that the membrane material can be securely fixed to the finger through its self-adhesive properties and does not fall off even after continuous bending (Fig. S6). The self-sealing strength of membranes was tested by adhering two pieces of $POCL_x$ membranes at one end with the other end being pulled till the connection between membranes completely disassembled (Fig. 3B and Fig. S7). $POCL_{10/15/20}$ membranes presented with significantly increased self-sealing strengths of 0.20 ± 0.02 MPa, 0.21 ± 0.01 MPa, and 0.25 ± 0.01 MPa, respectively, compared with POC (0.15 ± 0.01 MPa) (Fig. 3C). To adapt to the procedure of tendon injury implantation, $POCL_x$ membranes could be manually curved to form a tubular-shape which could maintain a self-sealed structure with an overlapped area (Fig. 3D and E). Despite the tubular form could be stable in dry atmospheric conditions, the environment of injured tendons is inevitably accompanied by watery conditions caused by transudate fluids. The strong hydrogen bonds introduced by LDI can induce the $POCL_x$ membrane to acquire strong and rapid self-sealing properties. To evaluate this property, the curved $POCL_x$ membranes were placed in sterile tubes and immersed in PBS to mimic the internal conditions of an

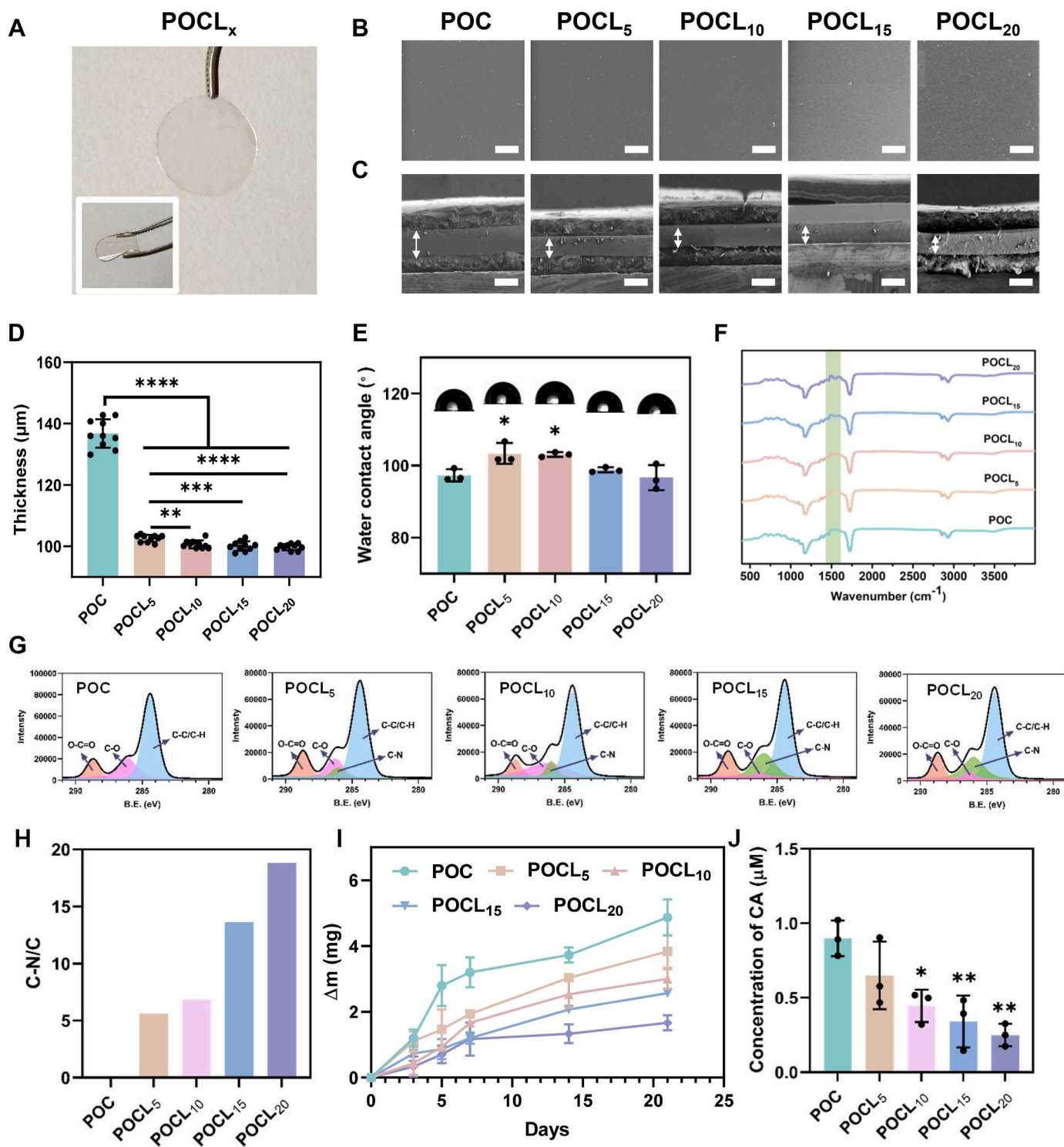


Fig. 2. Characterization of the citrate-based membranes. A) Gross view and flexibility of POCL_x membranes. SEM images of the B) surface (scale bar is 50 μm) and C) lateral view of POCL_x membranes (scale bar is 200 μm). White arrows demonstrate the thickness of the POCL_x membranes. D) Lateral thickness of the POCL_x membranes based on SEM images. E) Water contact angle of POCL_x membranes. F) FTIR spectra analysis of POCL_x membranes. G, H) XPS analysis and C-N/C ratio of POCL_x membranes. I) Degradation rate of POCL_x membranes in a duration of 21 days in degradation medium and J) concentration of CA in POCL_x membrane-immersed medium. Results are presented as means \pm SD. Statistical significance was calculated by one-way ANOVA. * $p < 0.05$, ** $p < 0.01$, *** $p < 0.001$, **** $p < 0.0001$.

injured environment (Fig. S8). 4 days following immersion, the overlapped area of pure POC membranes had loosened and the tubular structure was disorganized. However, with the support of strong hydrogen bonds, POCL_{5/10/15/20} membranes could consistently maintain the tubular structure (Fig. 3F). Intriguingly, the tubular structure

could be maintained up to 30 days within a wet environment (37 $^\circ\text{C}$, Fig. S9). Collectively, the data above corroborated that self-sealing properties of POCL_x membranes would simplify the handling of surgical implantation with non-suture fixation and structure maintenance.

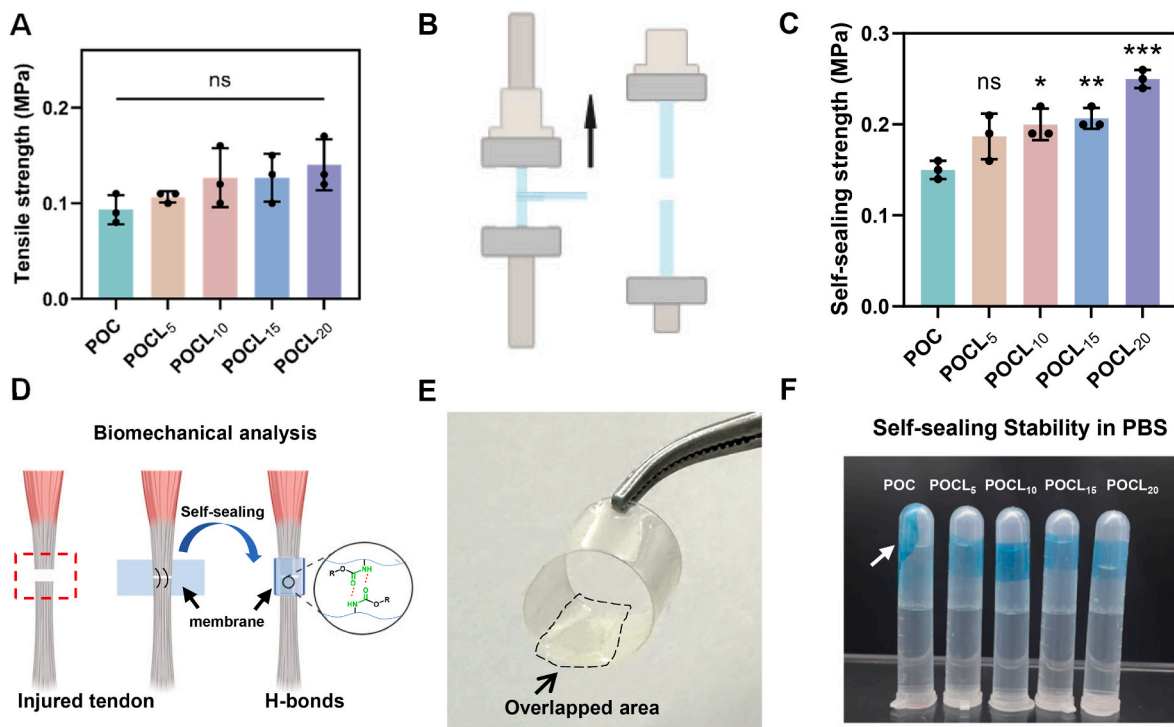


Fig. 3. Mechanical analysis and self-sealing evaluation of POCL_x membranes. A) Tensile strength of multiple POCL_x membranes. B) Schematic diagram and C) measurement of the self-sealing strength of POCL_x membranes. D) Schematic illustration of the application of POCL_x membranes and self-sealing capacity via strong hydrogen bonds. E) Image of the synthesized membrane curved into a tubular shape and structure maintained via an overlapped contact area. The dotted line shows the overlapped area of the membrane. F) Self-sealing stability of POCL_x membranes immersed in PBS for 4 days. White arrow indicates the detached membrane. Results are presented as means \pm SD. Statistical significance was calculated by one-way ANOVA. * $p < 0.05$, ** $p < 0.01$, *** $p < 0.001$, ns, non-significant.

2.3. Anti-biofouling and biocompatibility of citrate-based membranes

Anti-biofouling consists of the ability to prevent the adhesion of cells and proteins onto the surface of materials. Considering application on tendons, the anti-biofouling capacity can further extend to prevention of PAF (Fig. 4A). Anti-biofouling analysis was carried out by incubating BSA and fibroblasts onto POCL membranes, and rinse off excessive non-adhered particles before observation (Fig. 4B–E). POCL_{0/5/10/15} membranes exhibited with a minimum amount of BSA protein attachment. Conversely, POCL₂₀ membranes had significantly increased adhesion of BSA proteins (Fig. 4B and D). There was a resemblance in these results as fibroblasts were highly adhered to POCL₂₀ membranes, and approximately unattached to POCL_{0/5/10} membranes (Fig. 4C and E). This phenomenon could be attributed to the unique characteristics of LDI as a bio-based isocyanate. The POC membrane without LDI crosslinking has the fastest degradation rate in PBS and releases a larger amount of citric acid. This creates a slightly acidic environment, which affects cell viability and inhibits cell adhesion to the surface. The introduction of LDI can regulate the release rate of citric acid and enhance the biocompatibility of the membrane. Additionally, the introduction of LDI increases the hydrogen bond content of the membrane material, thereby improving its hydrophilicity. As a result, with the increase of LDI content, the anti-adhesive property of the membrane material decreases. This highlights the need to carefully balance the incorporation of LDI to optimize both biocompatibility and anti-fouling performance for practical applications. The biocompatibility of POCL_x membrane extractive fluids were further assessed on fibroblasts. Results showed that POC and POCL₅ membranes had a cell viability of roughly 50%, while the rest along with blank controls had a cell viability of over 70% (Fig. 4F). This verifies that POCL_x membranes reduce the adherence of cells via anti-biofouling capacities rather than direct cytotoxic effects. However, low crosslinking ratio of LDI does have lower biocompatibility to fibroblasts which accords with former degradation results. These results

can be further confirmed via cell live/dead staining, showing a significantly increased percentage of dead cells in POC groups compared with POCL_{5/10/15/20} incubation (Fig. 4G and Fig. S10). The low biocompatibility of POC could be mainly due to the intracellular concentration of CA. The results indicate that the POC and POCL₅ groups exhibited higher cytotoxicity due to the elevated release of citric acid from degradation. This led to cellular damage, which in turn caused a decrease in intracellular CA levels. However, as the degree of crosslinking increased, the biocompatibility of the membrane materials was enhanced. Consequently, the intracellular CA levels gradually rose and eventually showed no significant difference compared to the control group (Fig. S11). Moreover, cytoskeletal staining revealed a significantly decreased cell area when treated with POC and POCL₅ extracted fluids (Fig. 4H and Fig. S12). The acidic milieu formed by POC could disrupt the functions of cell cycle and cell spreading. Conclusively, low ratios of LDI crosslinking prevented biofouling, but also induced cell death. Meanwhile, higher ratios of LDI crosslinking improved the biocompatibility of cells and also increased biofouling. POCL₁₀ membranes, as the middle ratio, exhibited with both excellent anti-biofouling potential and good biocompatibility which were suitable for anti-adhesive implantation.

2.4. POCL₁₀ promotes TSPC proliferation and cell cycle processes

Resident TSPCs are responsive upon injury that proliferate and replace impaired tenocytes. To further explicit the impact of POCL_x membranes on the biocompatibility of stem cells, TSPCs were incubated in POCL_x extracted medium. Live/dead staining of TSPCs showed that POC medium-treated stem cells had an increased rate in cell death compared with non-treated control. In contrast, POCL₅ and POCL₁₀ medium-treated cells had significantly decreased death rates compared with control and POC. POCL₁₅ and POCL₂₀ had no significant difference compared with control (Fig. 5A and E). Cell viability analysis with CCK8

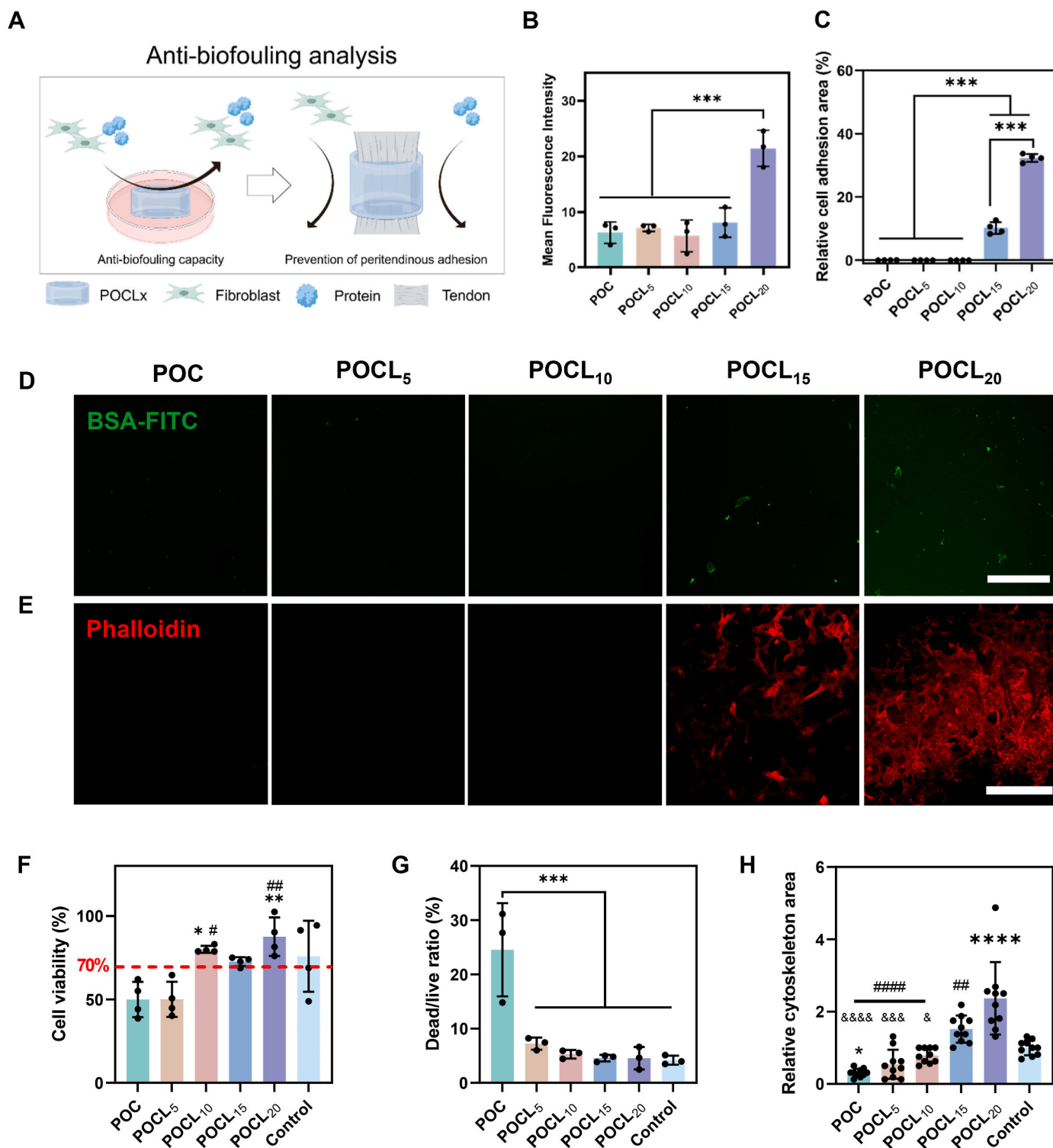


Fig. 4. Anti-biofouling evaluation and biocompatibility of POCLx membranes. A) Schematic diagram of the anti-biofouling analysis of POCLx membranes against cells and proteins that analogy to tendon application for anti-peritendinous adhesion. B) The mean fluorescence intensity and D) image of BSA-FITC adhesion on POCLx membranes. Scale bar is 200 μ m. C) Relative cell adhesion area and E) image of fibroblasts cultured on POCLx membranes stained by phalloidin. Scale bar is 500 μ m. F) CCK-8 analysis, Dead/live staining ratio and H) cytoskeletal area analysis of fibroblasts treated by POCLx immersed medium. Results are presented as means \pm SD. Statistical significance was calculated by one-way ANOVA. * $p < 0.05$, ** $p < 0.01$, *** $p < 0.001$, **** $p < 0.0001$. “***”, “#”, “&” represents the comparison between groups against CT, POC and POCL10, respectively.

confirmed these results. It further showed that proliferation rates treated by POCL₁₀ extracted medium were significantly increased compared with the other groups (Fig. 5B). The cytoskeleton area displayed that POC treated cells had a significantly smaller cell area, while it was

significantly increased in POCL₁₀ treated TSPCs (Fig. 5C and F). As TSPC biocompatibility and proliferation was closely related with the concentration of CA extracted from POCL_x membranes, we evaluated whether the incubation of TSPCs with different CA solutions, in

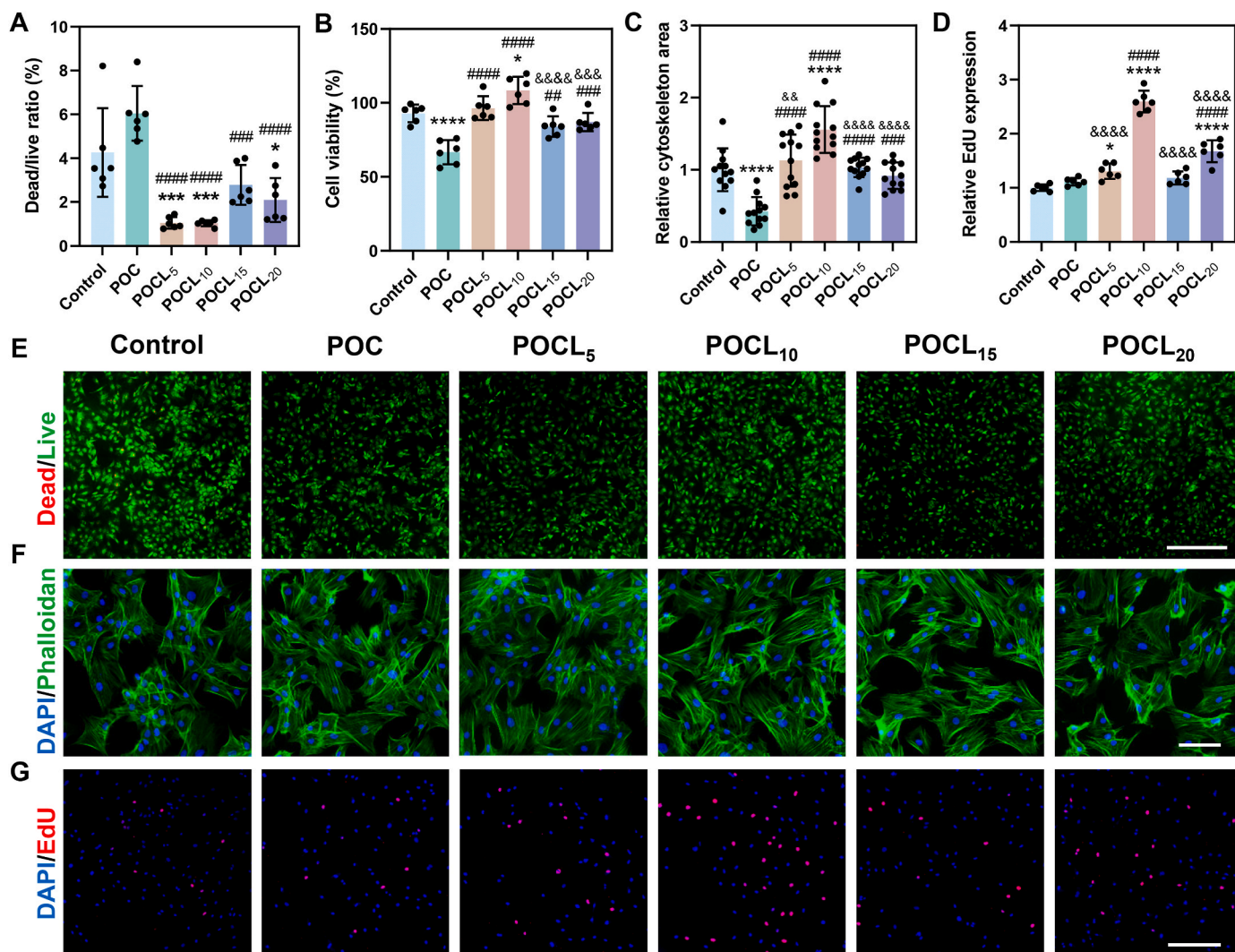


Fig. 5. Biocompatibility of POCLx membranes on TSPCs. A) Dead/Live ratio, B) CCK-8 analysis, C) cytoskeleton analysis and D) EdU expression of TSPCs treated by POCLx immersed medium. E) Dead/Live staining (scale bar is 500 μm), F) phalloidin staining (scale bar is 100 μm) and G) EdU staining (scale bar is 200 μm) of TSPCs treated by POCLx immersed medium. Results are presented as means ± SD. Statistical significance was calculated by one-way ANOVA. * $p < 0.05$, ** $p < 0.01$, *** $p < 0.001$, **** $p < 0.0001$. “*”, “#”, “&” represents the comparison between groups against CT, POC and POCL₁₀, respectively.

accordance with Fig. 2J, could promote the same outcome. The mean concentrations were selected as sodium citrate was resolved in cell culture medium to form 0.9 μM, 0.65 μM, 0.45 μM, 0.34 μM and 0.25 μM CA solutions, while normal culture medium (0 μM CA) was used as control. Results indicated that 0.9 μM CA treated TSPCs had a significantly lower cell viability and higher dead/live ratio compared with other concentrations. In line with extracted medium cultured results, 0.45 μM CA treatment could promote the cell viability of TSPCs which reflected the concentration of POCL₁₀ membranes (Fig. S13 and S14). These results have suggested that POCL₁₀ treatment had an enhanced influence on stem cell proliferation induced by citrate. Thus, EdU staining was carried out to directly assess the facilitation of POCL₁₀ on cell cycle processes. Results demonstrated that EdU expression of POCL₁₀ treatment was significantly upregulated compared with the other groups (Fig. 5D and G). Overall, POCL₁₀ membranes had great biocompatibility on TSPCs as well and could directly promote stem cell proliferation via exogenous citrate. In union with former anti-biofouling and mechanical results, POCL₁₀ was chosen for further pro-regenerative mechanistic assessments and in vivo studies.

2.5. Mechanistic investigation of the metabiotissugenic potential of POCL₁₀ on TSPCs

To further verify the underlying mechanism of how the POCL₁₀ membrane regulates the biological processes of TSPCs, we carried out a bulk RNA sequencing (RNAseq) analysis on TSPCs which were treated with PBS, POC and POCL₁₀, respectively (Fig. S15). The correlation of samples was analyzed through principal component analysis (PCA) and Pearson correlation analysis. POCL₁₀ treated TSPCs exhibited with a transcriptional differentiation compared with Control and POC groups (Fig. S16). Separately compared, 45 differentially expressed genes (DEGs) were detected in POC vs Control, 2380 DEGs in POCL₁₀ vs Control, and 2273 DEGs in POCL₁₀ vs POC (Fig. 6A and Fig. S17 and S18). GO enrichment analysis revealed a series of pathways, such as the developmental process, anatomical structure development, extracellular matrix, cell junction, cell population proliferation, cell differentiation, etc upregulated by POCL₁₀ treatment compared with both control and POC (Fig. 6B and Fig. S19A). Contrarily, GO enrichment of POC vs Control showed an increase in neutrophil, granulocyte and leukocyte chemotaxis (Fig. S19B). Gene set enrichment analysis (GSEA) showed that in POC vs Control, cells were transferred into an inflammatory responsive state with upregulated cell chemotaxis and downregulated

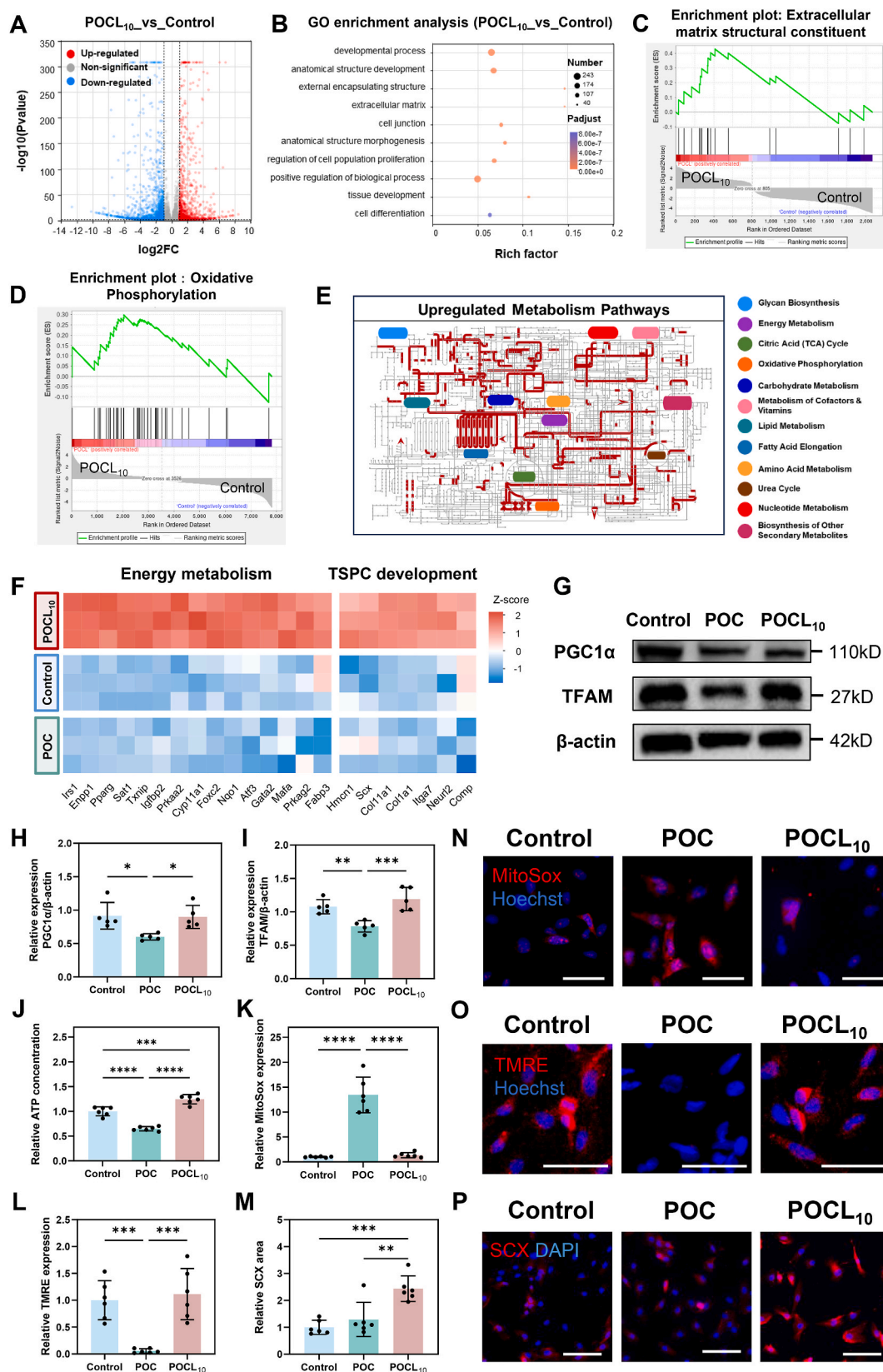


Fig. 6. RNaseq analysis of synthetic membranes on TSPCs. A) Volcano plot displaying DEGs between POCL10 and Control (non-treated) TSPCs in vitro. B) GO enrichment analysis of upregulated DEGs. C,D) GSEA of genes altered in POCL10 vs control. E) iPath analysis of upregulated metabolic genes between POCL10 and control. F) Heatmap of energy metabolism and TSPC development related genes. G–J) Western Blotting images of PGC1α, TFAM and β-actin. J) Relative ATP concentration of TSPCs. K,L,N,O) Mitochondrial function analysis of TSPCs using MitoSox and TMRE staining. Scale bar is 50 μm. M,P) SCX staining of TSPCs. Scale bar is 100 μm. Results are presented as means ± SD. Statistical significance was calculated by one-way ANOVA. *p < 0.05, **p < 0.01, ***p < 0.001, ****p < 0.0001.

mitotic cell cycle process (Fig. S20). Meanwhile, POCL₁₀-induced TSPC GSEA demonstrated with the upregulation of extracellular matrix structural constituent, oxidative phosphorylation, Notch signaling pathway, lysine degradation and NADH dehydrogenase activity pathways, while glycolysis/gluconeogenesis, inflammatory response and interleukin-6 production pathways were significantly downregulated (Fig. 6C, D and Fig. S21). Compared with POC, GSEA analysis further displayed that collagen fibril organization and SNARE complex pathways were highly upregulated under POCL₁₀ induction (Fig. S22). These results verified that POCL₁₀ had a better biocompatibility to TSPCs in accordance with former results, emerging with significantly increased OXPHOS function, cellular development and ECM formation.

As POCL₁₀ treatment induced the metabolic shift as OXPHOS pathways upregulated and glycolysis downregulated, the iPath metabolism analysis of POCL₁₀ upregulated genes was further evaluated. Results indicated that a majority of metabolism-related genes in glycan biosynthesis, energy metabolism (TCA cycle, oxidative phosphorylation), carbohydrate metabolism, lipid metabolism (fatty acid elongation), and amino acid metabolism (urea cycle) were upregulated (Fig. 6E). Pure POC treatment had few metabolic pathways upregulated compared with POCL₁₀ (Fig. S23). Energy metabolism-related genes and tendon development-related genes were compared within the three groups. Energy metabolism genes (*Fabp3*, *Prkag2*, *Mafa*, *Gata2*, *Atf3*, *Pparg* etc.) and TSPC development related genes (*Scx*, *Col1a1*, *Col11a1*, *Itga7*, etc.) were significantly upregulated by POCL₁₀ treatment (Fig. 6F). Additionally, genes correlated with the homeostasis of tendon stem cells (*Pdgfra*, *Bmp4*, etc.) were downregulated under POCL₁₀ induction (Fig. S24). This indicated that POCL treatment not only induced the metabolic shift of TSPCs from glycolysis to OXPHOS, but also induced stem cell development by changing its state from homeostasis to differentiation. Protein-protein interaction (PPI) network analysis further revealed that oxidative phosphorylation, cellular response to insulin stimulation, and AMPK signaling pathways are closely correlated with tendon development (Fig. S25).

To confirm the transcriptional results, western blotting of peroxisome proliferator-activated receptor Gamma, coactivator 1 alpha (PGC1 α) and transcription factor A, mitochondrial (TFAM) were processed, which are key energy metabolism-related proteins that function in mitochondrial biogenesis and oxidative metabolism [43]. The expression of both proteins significantly decreased under POC treatment, while POCL₁₀ had no significant difference with control (Fig. 6G–I). However, ATP concentration analysis revealed that POCL₁₀ treated TSPCs had increased ATP production compared to control. With decreased protein levels of PGC1 α and TFAM, POC significantly reduced ATP production (Fig. 6J). Mitochondrial superoxide assay (MitoSox) and mitochondrial membrane potential assay (TMRE) were conducted to further evaluate the mitochondrial functions of treated TSPCs [44]. Although POCL₁₀ had no significant difference with control, POC treatment exhibited with highly increased superoxides and impaired mitochondrial membrane potential (Fig. 6K, L, N and O). Furthermore, immunofluorescence of the TSPC marker, Scleraxis (SCX), revealed that POCL₁₀ extracted medium remarkably induced its expression (Fig. 6M and P). These results indicated that disturbed mitochondrial function and overexpressed superoxides led to POC-induced TSPC cell death. Meanwhile, POCL₁₀ treated TSPCs maintained regular mitochondrial functions with enhanced OXPHOS-mediated production of ATP for stem cell development. Collectively, POCL₁₀ could highly reprogram the metabolic processes within TSPCs, which further promotes the cellular processes of stem cell differentiation and verifies the metabotissugenic influence of POCL membranes.

2.6. POCL₁₀ prevents adhesion formation in vivo

Considering that the POCL₁₀ membrane has a good resistance against cell and protein adhesion in vitro, and also promotes the differentiation of TSPCs, POC and POCL₁₀ membranes were further applied to a rat

Achilles tendon injury model to assess its effect on PAF prevention and tendon regeneration. No treatment and commercial membrane implantation were respectively used as a negative and positive control for anti-biofouling comparison. On postoperative day 21, rats were euthanized and the healed tendon was grossly assessed. No infectious ulcers or necrosis were found. The blank control group presented with significant adhesion formation surrounding the tendon, making it difficult to separate the tendon from adjacent tissue with the detacher. In contrast, the POCL₁₀ group along with POC and the commercial Sefrafil group both showed significantly reduced PAF and the detacher passed between the tendon and adjacent tissue with low resistance (Fig. 7A). According to the gross assessment standards (Fig. S26), POC, POCL₁₀ and Sefrafil scores were significantly lower than control, and there was no significance between the two anti-adhesive membranes (Fig. 7D). This indicated that the POC and POCL₁₀ membranes could achieve the same anti-biofouling potential as the commercial membrane. All anti-adhesive membranes were still wrapped around the tendon surface by day 21, providing a physical barrier against the invasion of adhesive tissues. However, the POC and POCL₁₀ membranes exhibited with a fairly more intact feature than the commercial membrane, indicating its stable degradation capacity in vivo.

Moreover, hematoxylin-eosin (HE) and Masson's staining was applied to histologically analyze the extent of peritendinous adhesion and tendon healing. Results showed that a dense and adequate amount of fibrous tissue around the repaired tendon was observed in the control group. Via the application of the anti-adhesive membranes, PAF was significantly reduced and an interspace was retained around the Achilles tendon with POC and POCL₁₀ treatment (Fig. 7B). Histological scoring of peritendinous adhesion (Fig. S27) revealed that POC and POCL₁₀ scored significantly lower than that in control and Sefrafil (Fig. 7E). This provided evidence that POC and POCL₁₀ application can markedly restrain the formation of PAF tissue in accordance with previous anti-biofouling analysis.

2.7. POCL₁₀ promotes achilles tendon regeneration and biomechanical function

As TSPC related genes were significantly upregulated in vitro, we hypothesized that POCL₁₀ could improve intrinsic regeneration of tendon in vivo. To verify our hypothesis, histological scoring of tendon healing was addressed. Scoring standards included the assessment of collagen fiber organization, cell alignment, cell nucleus morphology, degenerative changes, vascularization and inflammation (Table S2). HE and Masson's staining of the normal tendon were used as a reference which scored 18 according to the grading system (Fig. S28). Tendon healing of the control group displayed with disorganized collagen deposition, randomized cell alignment, increased angiogenesis of large vessels and increased leukocyte infiltration. Conversely, with the implant of POCL₁₀ membrane, ECM was linearly organized and cells were orderly aligned, along with the regeneration of evenly distributed small vessels and inhibition of inflammation. The commercial anti-biofouling membrane and the POC membrane exhibited a similar tendon healing degree with blank controls accompanied with inflammation, nonlinear ECM formation and large vessel angiogenesis (Fig. 7C). Histological grading further supported the observed diversity (Fig. 7F). Via POCL₁₀ treatment, there was an improved tendon regeneration compared with non-treatment or application of commercial anti-adhesive membranes.

The biomechanical strength of the tendon is a major aspect that composes its biological function. It is associated with the outcome of better weight bearing which is the main function of tendons [45]. Thereby, the recovery of mechanical strength is a critical aspect when estimating tendon healing. Healed tendons were collected on postoperative day (POD) 21 for biomechanical analysis (Fig. S29). Important parameters as maximum load, stiffness and maximum strain were recorded and analyzed. Results detected that maximum strength and

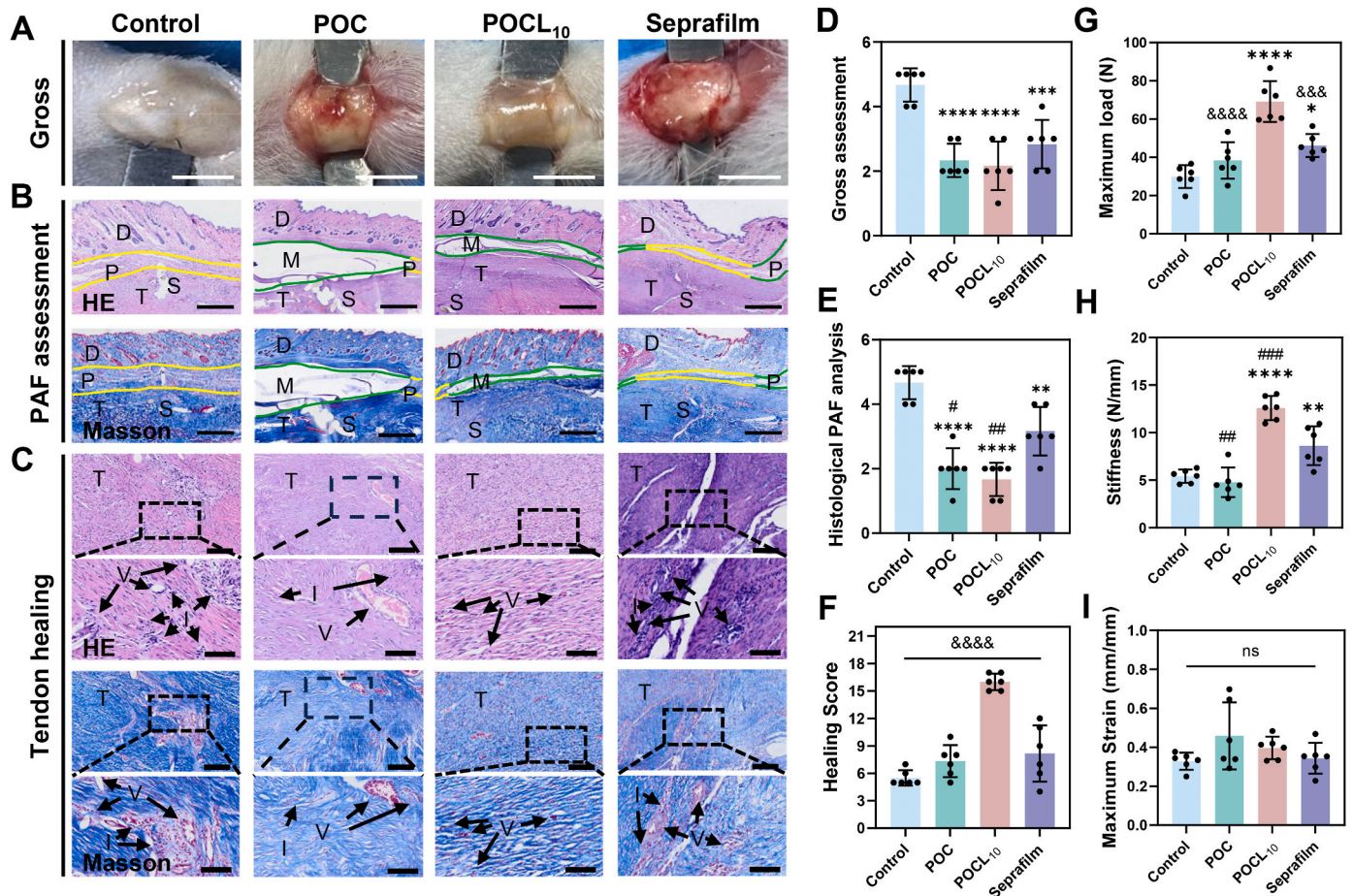


Fig. 7. Evaluation of intrinsic tendon regenerating efficacy of POCL10 membranes on tendon injury. A,D) Gross analysis of anti-peritendinous adhesion efficacy of implanted membranes and non-treated tendons. Scale bar is 3 mm. B,E) Histological PAF assessment of membranes. Scale bar is 1 mm. T, tendon; P, peritendinous adhesion; S, suture; D, dermis; M, membrane. C,F) Histological tendon healing assessment of regenerated tendons. Scale bar is 200 μ m and 100 μ m for original and enlarged images, respectively. T, tendon; V, vessels; I, inflammation. G-I) Biomechanical examination of regenerated Achilles tendons including, (G) maximum load, (H) stiffness and (I) maximum strain. Results are presented as means \pm SD. Statistical significance was calculated by one-way ANOVA. * p < 0.05, ** p < 0.01, *** p < 0.001, **** p < 0.0001, ns, non-significant. “*”, “#”, “&” represents the comparison between groups against Control, Seprafilm and POCL10, respectively.

stiffness of POCL₁₀ membrane treated tendons were approximately 2.3 folds higher than non-treatment and 1.5 folds higher than Seprafilm interference, respectively. POC treated tendons had no significant difference in mechanical strength compared with control (Fig. 7G and H). The maximum strain of regenerated tendons had no significant difference between different groups (Fig. 7I). These results indicated that POCL₁₀ membranes could significantly promote the toughness of regenerated tendons. Collectively, with the application of a metabolic regulating membrane could not only form a suitable anti-biofouling barrier, but also promote tendon regeneration to a greater extent and highly recover its crucial biophysiological functions.

2.8. POCL₁₀ induces TSPC proliferation and collagen deposition

The proliferation and differentiation of TSPCs happen days upon tendon injury to replace defected tenocytes and heal the impaired tissue. According to RNAseq results, the controlled release of citrate has a significant effect on promoting energy metabolism and differentiation of TSPCs. Therefore, immunofluorescence staining of key tendon differentiation markers, SCX and collagen type 1 (COL1), were conducted on regenerated tendon *in vivo*. There was a low expression level of SCX and COL1 in non-treatment, POC and Seprafilm groups POD 21, indicating a consecutive healing process was undergoing in the repairing site. However, application of POCL₁₀ membrane significantly prompted SCX and COL1 expression, showing highly activated intrinsic regeneration

properties compared with control, POC and commercial treatment (Fig. 8A, C and D). RNAseq results implied that inflammatory pathways were also reduced in POCL₁₀ treated groups. Thus, CD68 expression was observed and results indicated that infiltrated macrophages were significantly reduced after POCL₁₀ treatment (Fig. 8B and E). These results demonstrated that POCL₁₀ strongly facilitates intrinsic tendon regeneration via stimulation and activation of TSPC, while inflammation was reduced.

CA supplied by the POCL₁₀ membrane provided an energy metabolic substrate source that can be transmitted into stem cells and induce OXPHOS to produce an adequate amount of ATP for tissue repairment. During the early stage of tendon healing, inflammatory infiltration assists with the clearance of defected cells and tissue, but leads to an excessive expense of energy as well [30]. Therefore, ATP levels during POD 7 were significantly low in all anti-biofouling membrane implanted groups, indicating a large consumption of energy compared with control (Fig. S30). Conversely, ATP concentration on POD 21 was significantly upregulated by POCL₁₀ treatment in contrast to control, POC and Seprafilm (Fig. 8F). Considering that POCL₁₀ were modulus matched to contacting tissues and had a reprogrammed transcription to inhibit inflammatory responses, the consumption of energy in the POCL₁₀ group could be due to the induced proliferation and differentiation of TSPCs during the early inflammatory phase. Furthermore, with sustained degradation, stable *in vivo* structure, and significantly increased ATP production during the proliferative and remodeling stages,

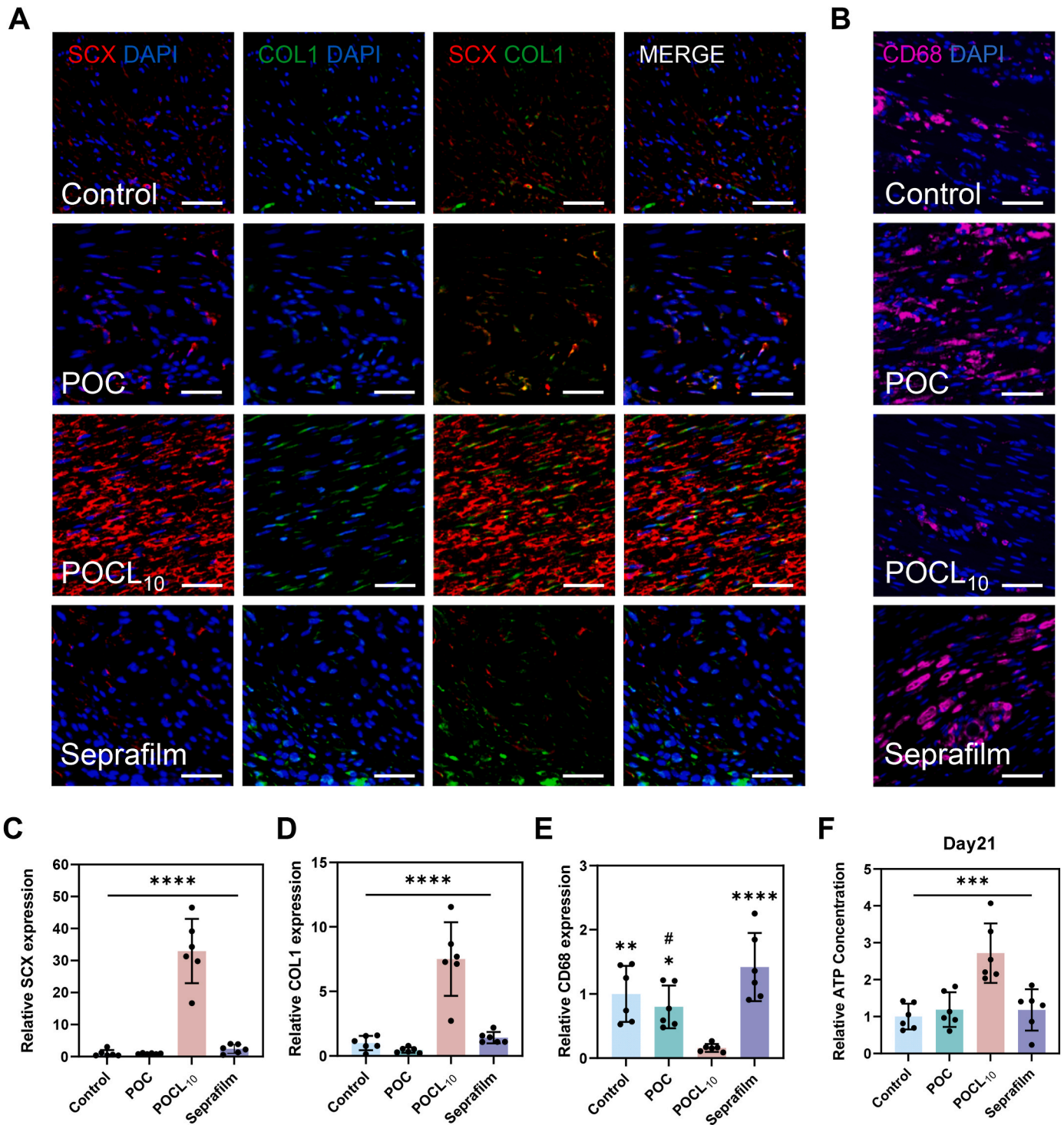


Fig. 8. Evaluation of TSPC expression, inflammation and energy metabolism in vivo. A) Immunofluorescence staining of SCX and COL1 on regenerated tendons. Scale bar is 50 μ m. B) Immunofluorescence staining of CD68. Scale bar is 50 μ m. C-E) Relative expression of SCX, COL1 and CD68. F) Relative ATP concentration of tendons among regenerating tendons on day 21 post-surgery. Results are presented as means \pm SD. Statistical significance was calculated by one-way ANOVA. * p < 0.05, ** p < 0.01, *** p < 0.001, **** p < 0.0001. “*”, “#”, “&” represents the comparison between groups against POCL10 and Seprafilm, respectively.

POCL₁₀-supplied CA could consistently facilitate the regeneration of tendon injury. Overall, POCL₁₀ demonstrated with a high potential to facilitate tendon regeneration via metabotendinogenesis.

2.9. Reliable biosafety and degradative properties of POCL₁₀

POCL membrane degradation and citrate release could enter the

bloodstream and flow through the body. Therefore, we collected visceral organs of rats 21 days after surgery. HE staining displayed that the heart, liver, spleen, lung and kidney remained intact and no pathological damage was caused by the deposition of POCL membranes (Fig. S31). Moreover, complete degradability of implanted materials is crucial for biosafety. Thus, the degradation duration of the POCL₁₀ membranes in vivo was further assessed. POCL₁₀ membranes were still found to be

intact 6 weeks post-operation with a thinner morphology consistent with the sustained degradation capacity *in vitro*. As in contrast, Seprafil™ had been fully degraded (Fig. S32). By week 9, POCL₁₀ membranes completely degraded *in vivo* verifying its good biocompatibility and sustainable degrading capacity (Fig. S33).

3. Conclusion

In conclusion, we introduce a metabotendinogenic membrane, POCL₁₀ with sustainable degradation, anti-biofouling capacity and favorable plasticity. POCL₁₀ membranes could be synthesized by a simple polycondensation method that consistently releases citrate and could be highly stable during surgical application. In accordance with anti-biofouling property against fibroblasts and proteins *in vitro*, POCL₁₀ successfully prevented PAF through *in vivo* implantation. Additionally, with the modified releasing rate of energy metabolic substrates, excellent biocompatibility to TSPCs was achieved exhibiting induced proliferation and cell cycle of stem cells. Mechanistically, citrate accumulation within TSPCs caused a metabolic shift from glycolysis to OXPHOS to provide an adequate amount of energy for stem cell development, ECM production and organization. Furthermore, in rat tendon injury models, POCL₁₀ induced long-term effects on tendons which obtained outstanding performance on ECM organization and enhanced mechanical functions to approximately 2.3 and 1.5 times greater than non-treatment and commercial treatment, respectively. Overall, this work establishes a metabotissugenic anti-biofouling platform to effectively achieve anti-peritendinous adhesion and stem cell development, providing a promising approach for intrinsic tendon regeneration upon injury and a novel approach for clinical treatment.

4. Experimental section

4.1. Synthesis and characterization of citrate-based membrane

Citric acid and 1,8-octanediol were added to a 50 mL round-bottom flask at a molar ratio of 1:1.1. The mixture was first dissolved at 160 °C for 20 min, followed by polymerization at 140 °C under 600 rpm stirring for 2 h. The resulting product was washed with deionized water 3–5 times and freeze-dried to obtain POC prepolymer. The Pre-POC was dissolved in anhydrous dioxane to form a 30 % (w/w) solution. Subsequently, 1 g of the solution was cross-linked with L-lysine diisocyanate (LDI) at mass ratios of 0 %, 5 %, 10 %, 15 % and 20 % to prepare membranes.

4.2. Characterization

The molecular structure of Pre-POC was observed by nuclear magnetic resonance spectroscopy (¹H NMR, AVANCE NEO, Bruker BioSpin, Switzerland). The morphologies and thickness of POCLs were observed by scanning electron microscopy (SEM, JSM-7500F, JEOL, Japan). The surface chemical compositions were investigated by X-ray photoelectron spectroscopy (XPS, Kratos AXIS-His, Shimadzu, Japan) equipped with Al K α X-ray source and attenuated total reflection Fourier transform infrared (ATR-FTIR) spectroscopy. The hydrophobicity of samples was measured by static water contact angle (WCA, OCA 25, Dataphysics, Germany).

4.3. *In vitro* degradation study

The POCL membranes were fabricated into small circular discs with a diameter of 6 mm. After weighing, the discs were placed in a phosphate-buffered saline (PBS, pH = 7.4) solution or esterase solutions (0.05 mg/mL), and subjected to oscillation in a shaking incubator at 37 °C. The discs were retrieved at 3, 5, 7, 14, 21 days, dried, and weighed again to record the changes in weight.

4.4. CA concentration measurement

CA concentration was tested with a Citric Acid Content Assay Kit (BC2150, Solarbio) according to the manufacturer's protocol. The medium of POCL_x immersed solution was retrieved. A working solution was prepared and mixed with the solution above. They were then incubated for 30 min before undergoing absorbance value analysis with a spectrophotometer at 545 nm. Intracellular CA concentration was estimated by primarily gathering incubated cell and ultrasound breaking cells walls before being mixed with the working solution.

4.5. Mechanical property testing

4.5.1. Tensile strength measurement

The POCL membranes were cut into a dumbbell shape with a length of 35 mm and a width of 2 mm in the middle using a mold. The ends were clamped and fixed with a length of 6 mm each. The sample was then stretched at a rate of 60 mm/min, and the relevant parameters, including tensile strength and elongation at break, were recorded.

4.5.2. Self-sealing strength measurement

The membrane material was fabricated into a rectangular shape with a width of 1.5 cm and a length of 4 cm. Two membranes were overlapped in a T-shape with an overlap length of 2 cm. The ends of the membranes were fixed in a tensile testing machine to measure the force required to completely separate the two membranes.

4.5.3. Self-sealing function analysis

The membrane was fabricated into a rectangular shape as above and curved to be attached by an overlapping area. Then membranes were placed into centrifuge tubes containing PBS and images of the membranes were taken on day 0 and until membranes were detached. To further evaluate the self-sealing potential of membranes around cylinder objects, membranes were wrapped around injecting syringes and placed in PBS, which was then incubated in a shaking incubator at 37 °C. Images of membranes were taken 30 days after immersion.

4.6. Anti-biofouling analysis against protein and cells

The POCL membranes were fabricated into small circular discs with a diameter of 8 mm. After thorough washing and sterilization, the discs were placed in a 48-well plate. FITC-BSA was prepared at a concentration of 2 mg/mL, and 200 μ L was added to each well. The samples were then co-incubated in a 37 °C incubator for 2 h. After incubation, the discs were removed, washed with PBS, and subsequently observed under a fluorescence microscope. Similarly, 10⁴ cells were seeded onto the surface of each membrane disc, followed by co-incubation for 24 h. After incubation, the discs were washed, stained, and observed. Immunofluorescence staining procedures are described below.

4.7. TSPC isolation and cell culture

All experiments were approved by the Institutional Animal Care and Use Committee (IACUC) of Shanghai Jiao Tong University. 4–6-week-old male Sprague-Dawley (SD) rats, weighing 200–250 g were used. The isolation of rat TSPCs was established as in previous studies [46]. In brief, the Achilles tendons were excised from healthy rats overdosed with 1 % sodium phenobarbital. Tissues were minced with sterile scissors and digested in 0.25 % trypsin (Gibco, USA) containing type I collagenase (3 mg/ml; Sigma-Aldrich) and passed through a 70 μ m cell strainer (Becton Dickinson) to yield single-cell suspension. Digestion was terminated with Dulbecco's modified Eagle medium/F12 (DMEM/F12), consisting of 10 % fetal bovine serum (FBS, Gibco, USA), 100 U ml⁻¹ penicillin (Gibco, USA), 100 mg/ml streptomycin (Gibco, USA) and 2 mM L-glutamine (complete culture medium) (Gibco, USA). The isolated cells were plated at low density (500 cells/cm²) and

cultured at 37 °C in a humidified incubator with 5 % CO₂ to form colonies. Culture medium was changed every 3 days. At day 14, TSPCs were trypsinized and mixed together as passage 0 (P0). TSPCs were cultured till they reached 80–90 % confluence. P4–6 TSPCs were used for all experiments. The NIH3T3 cells were cultured in DMEM containing 10 % of FBS, 100 mg/mL of streptomycin and 100 U mL⁻¹ of penicillin at 37 °C with 5 % CO₂ humidified atmosphere. When growing to 80 %, the cells were diluted to 1 × 10⁵ cell mL⁻¹.

4.8. Cell biocompatibility assessment

Fibroblasts (NIH3T3) and TSPCs were selected to evaluate the biocompatibility. The sterilized membranes (POC, POCL₅, POCL₁₀, POCL₁₅, POCL₂₀) were placed into 48 well plates with 1 mL culture medium, and incubated in the incubator for 24 h. In a 96-well plate, 100 µL of the cell suspension was added to each well. After co-incubation for 24 h, the medium was replaced with an equal volume of the material extract solution, and the incubation was continued for an additional 24 h. The cell viability was tested by CCK8 assay (Solarbio, China). 1 mL CCK8 was dissolved in 10 mL DMEM mixed solution. The original solution was replaced with the same volume of CCK8 solution, and then incubated in the incubator for 1 h in the dark. The absorbance value at 450 nm was determined after the whole plate was shaken evenly. Calcein/PI staining was supported by Calcein/PI Cell Viability/Cytotoxicity Assay Kit (Beyotime, China) and were used according to the manufacturer's protocol 24 h after incubation. Cell adhesion of cells was evaluated by staining Phalloidin/DAPI (Servicebio, China) 24 h after incubation.

4.9. RNA sequencing

TSPCs were treated with POC or POCL₁₀ extracted medium for 24h. Non-treatment wells were used as control. Cell samples were collected and sent to the Shanghai Majorbio Institute for sequencing. The data were analyzed on the online platform of Majorbio Cloud Platform and the difference between the two groups was analyzed by DESeq. DEGs were screened with a threshold of $|\log_2 \text{fold change}| > 1$ and $p < 0.05$.

4.10. Cellular immunofluorescence staining

TSPCs were seeded in 24-well plates and incubated with POCL_x extracted medium or vehicle control for 24 h as mentioned above. Subsequently, cells were fixed with 4 % paraformaldehyde for 10 min, permeabilized with 0.1 % Triton X 100 in TBS, blocked with 10 % normal goat serum (NGS, Jackson ImmunoResearch, USA) and then incubated with anti-SCX (1:500, ab58655, Abcam, UK) antibody at 4 °C overnight. Cell nucleus was stained with DAPI. Cell proliferation of TSPCs was evaluated with a BeyoClick EdU Cell Proliferation Kit (Beyotime, China) following the manufacturer's protocol. Briefly, EdU working solution was added to the culture medium and incubated for 2 h. Cells then underwent a same fixation and permeabilizing procedure as above. Subsequently, a click additive solution was added to the wells and incubated for 30 min. Cell nucleus was stained with Hoechst. The images were captured using fluorescence confocal microscopy (Leica DM6, Germany).

4.11. Western blotting

TSPCs were incubated with former POC and POCL₁₀ extracted medium for 24 h before being homogenized with RIPA lysis buffer containing protease inhibitor cocktail (Sigma-Aldrich, USA) to obtain proteins. Equal amounts of protein were separated by SDS-PAGE electrophoresis, transferred to PVDF membranes and blocked with 5 % milk before being incubated with PGC1 α , TFAM and β -actin (Beyotime, China) antibodies 4 °C overnight. Secondary antibody were subsequently incubated and blots were detected by chemiluminescence

system and their optical density was detected by ImageJ software.

4.12. Intracellular and tissue ATP concentration analysis

Intracellular and tissue ATP levels were determined in TSPCs and regenerated tendons by an Enhanced ATP Assay Kit (Beyotime, China) following manufacturer's protocol. The value in experimental group was normalized to that in vehicle control. TSPCs were treated with POCL₁₀ extracted medium prepared as above or vehicle control for 24 h, washed and harvested after mixing with nucleotide releasing buffer and incubated for 5 min at room temperature with gentle shaking. Tendon tissue samples were collected on day 7 and 21 post-operation and further lysed and homogenized before undergoing analysis. Sample were analyzed with a luminometer (BioTek Synergy HTX, USA).

4.13. Mitochondrial function analysis

TSPCs were incubated with former POC and POCL₁₀ extracted medium for 24 h before undergoing mitochondrial superoxide assay (MitoSox) and mitochondrial membrane potential assay (TMRE) (Beyotime, China) according to the manufacturer's protocol. Briefly, culture medium was removed and washed with PBS before adding the working medium of each assay kit. Cells were incubated for 30 min in a 37 °C incubator and working medium was washed. Hoechst was added to mark the cell nucleus. The images were captured using fluorescence confocal microscopy (Leica DM6, Germany).

4.14. Tendon injury (TI) model

All Sprague–Dawley (SD) rats were housed in isolated ventilated cages barrier facility at Shanghai Jiao Tong University Laboratory Animal Center. The mice were maintained on a 12/12-h light/dark cycle, 20–26 °C with sterile pellet food and water ad libitum. SD rats were randomly separated into four groups, which are control, POC, POCL₁₀ and Seprafilm, respectively. Following a previously reported protocol, a tenotomy model was created as the TI model [47]. Briefly, SD rats were anesthetized with pentobarbital sodium (30 mg kg⁻¹body weight). The hind limbs were disinfected before the posterior middle skin went through a 2 cm longitudinal incision to exposed the Achilles tendon. The tendon was cut in a transverse manner and was mended by a modified Kessler tendon suture. A 10 mm width and 20 mm length POC, POCL₁₀ membrane or Seprafilm (Baxter, USA) was wrapped around the injured tendons but nothing was applied in the control group. After the operation, rats were returned to the cage and kept warm under a baking lamp until awakening. Rats were euthanized at 4 time points (1 week, 3 weeks, 6 weeks and 9 weeks after surgery). Tissues collected at 1 week were used for examining in vivo ATP concentration of tendon tissue ($n = 3$ for each group). Tissues collected at 3 weeks were used for estimating the anti-biofouling and pro-regenerative capacity of membranes, along with biomechanical analysis and in vivo ATP concentration ($n = 9$ for each group), as injured tendons have repaired and formed peritendinous adhesions by this period. This time point is optimal for grading healing and anti-biofouling rates. Tissues collected at 6 and 9 weeks were used for estimating the anti-biofouling and in vivo degeneration capacity of membranes ($n = 3$ for each group). All grading procedures were assessed using the grading scales described below by individuals blinded to treatment allocation.

4.15. Histological staining

The collected tissues were fixed in a general tissue fixative overnight and hind limbs underwent decalcification until tibia bones were easily penetrable with needles. Tissue paraffin blocks were prepared, and 4 µm-thick sections were obtained. HE staining followed the standard protocol for assessing PA severity and healing. Masson staining was used for collagen deposition and ECM fiber organization evaluation.

4.16. Assessment of adhesion by gross observations and histological evaluation

Gross observations were graded according to the following classification criteria (Fig. S26, Supporting Information). Grade 1: no adhesion; grade 2: blunt dissection; grade 3: less than 50 % area requiring sharp dissection; grade 4: 50–97.5 % area requiring sharp dissection; grade 5: over 97.5 % area requiring sharp dissection, respectively. Histological severity of PA was assessed using an adhesion scoring system (Fig. S27, Supporting Information). Grade 1: no adhesion; Grades 2–5: <25 %, 25–50 %, 50–75 %, and >75 % adhesion areas in the gap between the tendon and peritendinous tissues, respectively.

4.17. Assessment of tendon healing

Histological tendon healing was scored according to a previous study and is described in Table S2, supporting information. Tendons were valued by assessing collagen/ECM organization, cell alignment, cell nucleus morphology, degenerative change/tissue metaplasia, vascularization and inflammation. A normal Achilles tendon scored 18 points using this scale.

4.18. Biomechanical evaluation

The biomechanical parameters of the healed tendons including the stiffness (N/mm), maximum load (N), and maximum strain (mm/mm) were recorded with a rheometer (Instron 5569, USA). Proximal and distal ends of each tendon was fixed with nonslip clamps attached to the rheometer. At a speed of 20 mm/min, tendons were pulled until terminal rupture.

4.19. Immunofluorescence staining

Immunofluorescence of SCX antibody (1:500, ab58655, Abcam, USA), Col1 antibody (1:200, AF6524, Beyotime, China), and CD68 antibody (1:500, AG1516, Beyotime, China) were performed on 4-mm formalin-fixed, paraffin-embedded tissue sections. Primary antibody was visualized by using tyramide signal amplification linked to a specific fluorochrome including fluorescein isothiocyanate, Cy3 or Cy5 for each primary antibody (all from Invitrogen, USA). For co-staining, a stripping procedure with microwave heating was performed between unifix immunofluorescence staining. The images were captured using fluorescence confocal microscopy (Leica DM6, Germany).

4.20. Statistical analysis

Each experiment contained at least three duplicates and presented as mean \pm standard deviation (mean \pm SD). Origin (version 2019b, MA, USA) and GraphPad Prism (version 8.0.2, CA, USA) were used to process, analyze and graph the collected data. To determine statistical significance between two groups, a *t*-test was utilized, while for multiple groups, one-way ANOVA was employed. The levels of significance were marked as follows: “*” for $p < 0.05$, “**” for $p < 0.01$, “***” for $p < 0.001$ and “****” for $p < 0.0001$.

CRedit authorship contribution statement

Changhao Han: Writing – original draft, Visualization, Methodology, Investigation, Formal analysis. **Lujiao Zhang:** Writing – original draft, Methodology, Investigation, Conceptualization. **Rong Bao:** Methodology, Investigation. **Yutong Lu:** Methodology, Investigation. **Xinpeng Dong:** Investigation. **Tianyi Zhang:** Methodology, Investigation. **Yuanhao Yang:** Methodology, Investigation. **Yao Xiao:** Methodology. **Liangxuan Fu:** Investigation. **Pusheng Guo:** Investigation. **Jian Yang:** Writing – review & editing, Supervision, Resources, Methodology, Conceptualization. **Shen Liu:** Writing – review & editing,

Supervision, Resources, Project administration, Methodology, Conceptualization.

Ethics approval and consent to participate

This study was performed in accordance with the recommendations in the Guide for the Care and Use of Laboratory Animals and relevant Chinese laws and regulations. The protocol was approved by the Institutional Animal Care and Use Committee (IACUC) of Shanghai Jiao Tong University, the Animal Protocol number is A2025046.

Declaration of competing interest

Jian Yang is an editor-in-chief for Bioactive Materials and was not involved in the editorial review or the decision to publish this article. All authors declare that there are no competing interests.

Acknowledgements

H.C. and Z.L. contributed equally to this study. The authors also thank FigDraw for the help in the preparation of the schematic diagram (Fig. 4a). This work was supported by National Key R&D Program of China (2024YFA1107800), National Natural Science Foundation of China (Grant No. 52403205, 82172408, 82425035 and 9236810338), Shanghai Jiao Tong University Medical College “Two-hundred Talent” Program (No.20191829), Program of Shanghai Academic/Technology Research Leader (No. 22XD1422600) and Shanghai Municipal Health Commission (No. 2022YQ073), The Second Three-Year Action Plan for Promoting Clinical Skills and Clinical Innovation in Municipal Hospitals of Shanghai Shengkang (No. SHDC2020CR4032), Original Exploration project of Shanghai Science and Technology Innovation Action Plan (No. 22ZR1480300), Shanghai “Medical Star” Young Medical Talent Training Funding Program (Outstanding Youth) and Shanghai Health Commission Health Industry Research Project (Excellent Project), Shanghai Municipal Health Commission Research Project (No. 20234Z0008) and Foundation of Muyuan Laboratory (Program ID: 13166022401).

Appendix A. Supplementary data

Supplementary data to this article can be found online at <https://doi.org/10.1016/j.bioactmat.2025.05.020>.

References

- [1] T.T. Huttunen, et al., Acute achilles tendon ruptures: incidence of injury and surgery in Sweden between 2001 and 2012, *Am. J. Sports Med.* 42 (10) (2014) 2419–2423.
- [2] U. Sheth, et al., The epidemiology and trends in management of acute Achilles tendon ruptures in Ontario, Canada: a population-based study of 27 607 patients, *Bone Joint Lett. J* 99-b (1) (2017) 78–86.
- [3] A. Ganestam, et al., Increasing incidence of acute Achilles tendon rupture and a noticeable decline in surgical treatment from 1994 to 2013. A nationwide registry study of 33,160 patients, *Knee Surg. Sports Traumatol. Arthrosc.* 24 (12) (2016) 3730–3737.
- [4] B. Kheilnezhad, A. Hadjizadeh, A review: progress in preventing tissue adhesions from a biomaterial perspective, *Biomater. Sci.* 9 (8) (2021) 2850–2873.
- [5] M. Mejias, et al., CPEB4 increases expression of PFKFB3 to induce glycolysis and activate mouse and human hepatic stellate cells, promoting liver fibrosis, *Gastroenterology* (New York, N. Y., 1943) 159 (1) (2020) 273–288.
- [6] X. Zhao, et al., Metabolic regulation of dermal fibroblasts contributes to skin extracellular matrix homeostasis and fibrosis, *Nat. Metab.* 1 (1) (2019) 147–157.
- [7] S.P. Magnusson, H. Langberg, M. Kjaer, The pathogenesis of tendinopathy: balancing the response to loading, *Nat. Rev. Rheumatol.* 6 (5) (2010) 262–268.
- [8] Y.P. Kato, et al., Mechanical properties of collagen fibres: a comparison of reconstituted and rat tail tendon fibres, *Biomaterials* 10 (1) (1989) 38–42.
- [9] S.J. Kew, et al., Regeneration and repair of tendon and ligament tissue using collagen fibre biomaterials, *Acta Biomater.* 7 (9) (2011) 3237–3247.
- [10] J.G. Snedeker, J. Foolen, Tendon injury and repair - a perspective on the basic mechanisms of tendon disease and future clinical therapy, *Acta Biomater.* 63 (2017) 18–36.
- [11] Y. Jiang, et al., Smart hydrogel-based trends in future tendon injury repair: a review, *Int. J. Biol. Macromol.* 282 (Pt 5) (2024) 137092.

- [12] Z. Tao, et al., Sustainable immunomodulatory via macrophage P2Y12 inhibition mediated bioactive patches for peritendinous antiadhesion, *Adv. Sci. (Weinh.)* 12 (4) (2025) e2409128.
- [13] G. Pan, et al., Full-course inhibition of biodegradation-induced inflammation in fibrous scaffold by loading enzyme-sensitive prodrug, *Biomaterials* 53 (2015) 202–210.
- [14] C. Huang, D.C. Ding, Outcomes of adhesion barriers in gynecologic surgeries: a retrospective study at a medical center, *Medicine (Baltim.)* 98 (50) (2019) e18391.
- [15] S. Avital, et al., Preventing intra-abdominal adhesions with polylactic acid film: an animal study, *Dis. Colon Rectum* 48 (1) (2005) 153–157.
- [16] V.W. Fazio, et al., Reduction in adhesive small-bowel obstruction by Sefrapilum adhesion barrier after intestinal resection, *Dis. Colon Rectum* 49 (1) (2006) 1–11.
- [17] J.C. Middleton, A.J. Tipton, Synthetic biodegradable polymers as orthopedic devices, *Biomaterials* 21 (23) (2000) 2335–2346.
- [18] E. Pişkin, Biodegradable polymers as biomaterials, *J. Biomater. Sci. Polym. Ed.* 6 (9) (1995) 775–795.
- [19] H. Tian, et al., Biodegradable synthetic polymers: preparation, functionalization and biomedical application, *Prog. Polym. Sci.* 37 (2) (2012) 237–280.
- [20] S. McMahon, et al., Bio-resorbable polymer stents: a review of material progress and prospects, *Prog. Polym. Sci.* 83 (2018) 79–96.
- [21] J. Yang, A.R. Webb, G.A. Ameer, Novel citric acid-based biodegradable elastomers for tissue engineering, *Adv. Mater.* 16 (6) (2004) 511–516.
- [22] H. Xu, et al., Citric acid: a nexus between cellular mechanisms and biomaterial innovations, *Adv. Mater.* 36 (32) (2024) e2402871.
- [23] A.K. Jha, et al., Network integration of parallel metabolic and transcriptional data reveals metabolic modules that regulate macrophage polarization, *Immunity (Camb., Mass.)* 42 (3) (2015) 419–430.
- [24] J. Zhu, C.B. Thompson, Metabolic regulation of cell growth and proliferation, *Nat. Rev. Mol. Cell Biol.* 20 (7) (2019) 436–450.
- [25] I. Martínez-Reyes, N.S. Chandel, Mitochondrial TCA cycle metabolites control physiology and disease, *Nat. Commun.* 11 (1) (2020) 102.
- [26] W.M. Taylor, M.L. Halperin, Regulation of pyruvate dehydrogenase in muscle. Inhibition by citrate, *J. Biol. Chem.* 248 (17) (1973) 6080–6083.
- [27] K.H.G. Verschuuren, et al., Structure of ATP citrate lyase and the origin of citrate synthase in the Krebs cycle, *Nature* 568 (7753) (2019) 571–575.
- [28] C. Ma, et al., Citrate-based materials fuel human stem cells by metabolic regulation, *Proc. Natl. Acad. Sci. U. S. A.* 115 (50) (2018) E11741–e11750.
- [29] C.E. Meacham, A.W. DeVilbiss, S.J. Morrison, Metabolic regulation of somatic stem cells in vivo, *Nat. Rev. Mol. Cell Biol.* 23 (6) (2022) 428–443.
- [30] J. Loeffler, et al., The metabolic microenvironment steers bone tissue regeneration, *Trends Endocrinol. Metabol.* 29 (2) (2018) 99–110.
- [31] L.P. Bechmann, et al., The interaction of hepatic lipid and glucose metabolism in liver diseases, *J. Hepatol.* 56 (4) (2012) 952–964.
- [32] S.A. Eming, T.A. Wynn, P. Martin, Inflammation and metabolism in tissue repair and regeneration, *Science* 356 (6342) (2017) 1026–1030.
- [33] Y. Yoshimoto, Y. Oishi, Mechanisms of skeletal muscle-tendon development and regeneration/healing as potential therapeutic targets, *Pharmacol. Ther.* 243 (2023) 108357.
- [34] K. Zhang, et al., Modulating glucose metabolism and lactate synthesis in injured mouse tendons: treatment with dichloroacetate, a lactate synthesis inhibitor, improves tendon healing, *Am. J. Sports Med.* 46 (9) (2018) 2222–2231.
- [35] Z. Ge, et al., Programmable DNA hydrogel provides suitable microenvironment for enhancing TSPCS therapy in healing of tendinopathy, *Small* 19 (32) (2023) e2207231.
- [36] Y. Wang, et al., Functional regeneration and repair of tendons using biomimetic scaffolds loaded with recombinant periostin, *Nat. Commun.* 12 (1) (2021) 1293.
- [37] D. Santini, et al., Aprepitant for management of severe pruritus related to biological cancer treatments: a pilot study, *Lancet Oncol.* 13 (10) (2012) 1020–1024.
- [38] X. Chen, et al., Mesenchymal stem cell therapy in severe COVID-19: a retrospective study of short-term treatment efficacy and side effects, *J. Infect.* 81 (4) (2020) 647–679.
- [39] P.T. Yin, et al., Stem cell-based gene therapy activated using magnetic hyperthermia to enhance the treatment of cancer, *Biomaterials* 81 (2016) 46–57.
- [40] M. Kamaraj, et al., Granular porous nanofibrous microspheres enhance cellular infiltration for diabetic wound healing, *ACS Nano* 18 (41) (2024) 28335–28348.
- [41] J.H. Shin, J.A. Han, Influence of casting variables on release kinetics of orally disintegrating film, *Foods* 13 (9) (2024).
- [42] P. Moshayedi, et al., The relationship between glial cell mechanosensitivity and foreign body reactions in the central nervous system, *Biomaterials* 35 (13) (2014) 3919–3925.
- [43] R.C. Scarpulla, Transcriptional paradigms in mammalian mitochondrial biogenesis and function, *Physiol. Rev.* 88 (2) (2008) 611–638.
- [44] K.H. Tsui, et al., Disruption of mitochondrial homeostasis with artemisinin unravels anti-angiogenesis effects via auto-paracrine mechanisms, *Theranostics* 9 (22) (2019) 6631–6645.
- [45] P. Eliasson, T. Andersson, P. Aspenberg, Rat Achilles tendon healing: mechanical loading and gene expression, *J. Appl. Physiol.* 107 (2) (1985) 399–407, 2009.
- [46] M. Ni, et al., Engineered scaffold-free tendon tissue produced by tendon-derived stem cells, *Biomaterials* 34 (8) (2013) 2024–2037.
- [47] Y. Li, et al., Sustained release of dicumarol via novel grafted polymer in electrospun nanofiber membrane for treatment of peritendinous adhesion, *Adv. Healthcare Mater.* 12 (15) (2023) e2203078.